RSC Advances

ROYAL SOCIETY OF CHEMISTRY

www.rsc.org/advances

Cite this: DOI: 10.1039/c0xx00000x

www.rsc.org/xxxxxx

ARTICLE TYPE

Construction of Au@$NaYF_4$:Yb^{3+},Er^{3+}/Ho^{3+} bifunctional hybrid nanocomposites with upconversion luminescence and photothermal properties

Yan Song,[a] Guixia Liu,*[a] Xiangting Dong,[a] Jinxian Wang,[a] Wensheng Yu,[a] Jingmei Li[b]

Received (in XXX, XXX) Xth XXXXXXXXX 20XX, Accepted Xth XXXXXXXXX 20XX
DOI: 10.1039/b000000x

Bifunctional hybrid nanocomposites based on upconversion luminescence and photothermal properties have a wide range of applications, especially biomedical diagnosis and therapy. Herein, the hybrid nanocomposites were prepared via combining $NaYF_4$:Yb^{3+},Er^{3+}/Ho^{3+} nanocrystals as shell layer materials and Au nanoparticles as core. The as-prepared nanocomposites can simultaneously take advantages of both upconversion luminescence of $NaYF_4$:Yb^{3+},Er^{3+}/Ho^{3+} nanocrystals and photothermal transduction property of Au nanoparticles. The structure, morphology and composition of nanocomposites were confirmed by X-ray powder diffraction (XRD), transmission electron microscopy (TEM) and energy dispersive spectroscopy (EDS). In addition, the upconversion luminescence and photothermal transduction were evaluated. We observed the overlap between the absorption band of Au nanoparticles and the upconversion emission peaks of the Er^{3+}/Ho^{3+} ions, and the luminescence resonance energy transfer (LRET) was researched and demonstrated. Under 980 nm laser irradiation, the upconversion luminescence and efficient photothermal transduction of the hybrid nanocomposite were found. Moreover, the bifunctional nanocomposites have also shown excellent biocompatibility.

1 Introduction

In recent years, lanthanide doped upconversion nanocrystals have attracted considerable research attention due to their unique optical properties and attractive potential applications in many fields, such as color displays, solid state lasers and solar cells.[1-3] Typical upconversion widely employed to convert near infrared radiation into visible light, refers to the nonlinear optical process, where the sequential absorption of low-energy pump multi-photons leads to the emission of the high-energy photons at a wavelength shorter than that of the excitation. The near infrared excitation wavelength lies in an optically transparent window for biological tissues with promising low radiation damage and high penetration depth for in vivo applications[4, 5]. Therefore, upconversion luminescence nanocrystals pumped by near infrared are expected to be a promising new generation of luminescence materials for investigation in the fields of biology and medicine.[6, 7] Lanthanide doped upconversion nanocrystals have obvious advantages, including low toxicity, sharp emission peaks, long emission lifetimes, higher photochemical stability, and minimum auto-fluorescence background compared with conventional semiconductor quantum dots and organic dyes.[8, 9] Among photoluminescent upconversion materials, fluoride nanocrystals have been reported as the outstanding upconversion matrixes due to low phonon energy, high luminous efficiency and high chemical stability.[10] As a desirable upconversion host, $NaYF_4$ nanocrystals have been used for efficient infrared-to-visible conversion via Er^{3+}/Ho^{3+} ions doped. To increase the near infrared absorption strength of upconversion material, Yb^{3+} ions are commonly used as effective sensitizers for the upconversion process and give an efficient excitation band around 980 nm.[4, 11] Hence, Yb^{3+}, Er^{3+}/Ho^{3+} co-doped $NaYF_4$ upconversion nanocrystals are suitable for luminescence imaging.[12]

Noble metal nanoparticles have attracted particular interest and extensive research owning to their interesting plasmonic properties. The localized surface plasmon resonance of Au nanocrystals is the most intriguing property.[13, 14] Au nanocrystals have the ability to sustain collective oscillation of the conduction electrons confined to the nanocrystals surface. This unique capability can significantly alter the electromagnetic field around the Au nanocrystals. Meanwhile, Au nanocrystals can possess large light scattering and absorption. The electromagnetic field near the surface of Au nanoparticles is very strong, which can change fluorescence and Raman signals of nearby molecules. So that the Au nanocrystals are widely used for ultrasensitive detection in chemistry and biomedical diagnostics.[15] In addition, Au nanoparticles have efficient photothermal transduction property, which is a fascinating ability of converting light to heat, due to surface plasmon resonance or energy transfer band. In this case, Au nanoparticles are very good candidates for photothermal therapy in medicine.[16, 17] Simultaneously, it is an emerging field with the potential to have a positive effect on human healthcare.

When the luminescence nanocrystals are placed in close proximity to the noble metal nanoparticles, the luminescence can be affected.[18-20] Previously, there have been a number of reports

involving the construction of hybrid nanostructure by combining lanthanide doped luminescence materials and noble metal nanoparticles.[21-25] It is reported that photoluminescence emission enhancement or quenching can be achieved via introduction of the Au nanoparticles, which depends on the spacing distance between the luminescence material and the Au nanoparticles.[26-29] The possible reason for the luminescence emission enhancement is generally attributed to an increase of the excitation rate by the local field enhancement or an enhancement of radiative decay rate by coupling the surface plasmon resonance and luminescence emission.[30-32] The quenching of luminescence may occur by non-radiative energy transfer from the luminescence material to the Au nanoparticles.[33-36] This energy transfer could be utilized for bioassays, biosensing, bioimaging, and photodynamic therapy via using promising lanthanide doped nanoparticles served as energy emitter and Au nanoparticles as energy quencher, respectively.[37, 38] As emitter, the upconversion luminescence nanoparticles have been recognized particularly as a highly sensitive and powerful tool in biomedical field.

In this work, we designed a facile solution route to synthesize a hybrid nanostructure combining $NaYF_4$:Yb^{3+},Er^{3+}/Ho^{3+} nanocrystals and Au nanoparticles as energy donor-acceptor pairs. The energy transfer may be occurred from the $NaYF_4$:Yb^{3+}, Er^{3+}/Ho^{3+} nanocrystals to Au nanoparticles in the hybrid nanostructure. The upconversion luminescence and luminescence resonance energy transfer (LRET) process of the hybrid nanocomposites were studied by investigated the upconversion luminescence intensity under the different pumping powers. The upconversion luminescence and efficient photothermal transduction of the hybrid nanocomposites are presented under excitation from a 980 nm laser. In addition, the biocompatibility of the Au@$NaYF_4$:Yb^{3+},Er^{3+} nanocomposite is also evaluated by the cytotoxicity assay. It is expected that the bifunctional hybrid nanocomposite could realize upconversion imaging and photothermal therapy in the biomedical fields.

2 Experimental section

Chemicals

As starting materials, Y_2O_3 (99.99%), Yb_2O_3 (99.99%), Er_2O_3 (99.99%), Ho_2O_3 (99.99%), NH_4F, HNO_3, sodium citrate and ethanol were purchased from Sinopharm Chemical Reagent Co., Ltd. Gold chloride tetrahydrate ($HAuCl_4$) and cetyltrimethylammonium bromide (CTAB) were purchased from Aladdin. The water used was deionized (DI). All other chemical reagents in this investigation were of analytical grade and were used without further purification.

Rare earth nitrate stock solutions were obtained by dissolving the corresponding rare earth oxides in dilute HNO_3 under heating with agitation followed by evaporating the solvent.

Synthesis of Au nanoparticles

In a typical synthesis, 0.025 mmol of $HAuCl_4$ aqueous solution was added into 45 mL DI water with 1 g CTAB to form bright yellow solution, which was vigorously stirred and heated to boil. Then, the 5 ml aqueous solution of sodium citrate (24.5 mg) was rapidly injected into the boiling $HAuCl_4$ aqueous solution under vigorous stirring. The solution was maintained refluxing and vigorously stirred until to appear wine red for 15 min. The solution was cooled to room temperature, centrifuged at 10000 rpm for 15 min. The supernatant was decanted. The precipitate was redispersed in 25 mL of DI water for further use.

Synthesis of the Au@$NaYF_4$:Yb^{3+},Er^{3+}/Ho^{3+} nanocomposites

The gold colloidal solution (5 ml) was diluted with DI water to 20 ml. Afterwards, sodium citrate solution (0.25 mmol) was injected into the solution and magnetic stirred for 30 min. A total of 0.25 mmol of $Y(NO_3)_3$, $Yb(NO_3)_3$ and $Er(NO_3)_3$ (molar ratio Y : Yb : Er = 78 : 20 : 2) were added into above solutions at room temperature. Subsequently, 0.24 mmol NH_4F was introduced. After stirring for 3 h, the mixture was collected by centrifugation at 8000 rpm for 5 min, washed with DI water and ethanol for several times, at last, the Au@$NaYF_4$:Yb^{3+},Er^{3+} nanocomposites were obtained. The Au@$NaYF_4$:Yb^{3+},Ho^{3+} nanocomposites were prepared by the same procedure. Meanwhile, the synthesis of the pure $NaYF_4$:Yb^{3+},Er^{3+} and $NaYF_4$:Yb^{3+},Ho^{3+} nanocrystals as comparative experiment were completed at the same conditions of Au@$NaYF_4$:Yb^{3+},Er^{3+}/Ho^{3+} shell encapsulation.

Characterizations

The sizes and morphologies of Au nanoparticles and Au@$NaYF_4$:Yb^{3+},Er^{3+} nanocomposites were examined by using a JEOL JEM-2010 transmission electron microscope (TEM) under a working voltage of 200 kV. The energy-dispersive spectroscopic (EDS) analysis was performed using an Oxford INCA energy system operated at 200 kV. The structure and phase composition of the as-synthesized samples were examined by X-ray powder diffraction (XRD) using a Bruker D8 FOCUS with Cu Kα radiation (λ= 1.54056 Å). The UV-Vis absorption spectra were acquired by a Shimadzu UV-2450 spectrophotometer. The upconversion emission spectra were recorded using a Hitachi F-7000 fluorescence spectrophotometer at room temperature coupled with a 980 nm laser source. The aqueous solution temperature was recorded using a HT3500C sensitive thermometer. The aqueous solutions of the samples were placed in a quartz cell and irradiated with a 980 nm near-infrared laser at power density of 1.2 W/cm^2 for 10 min.

Cytotoxicity assay

The cytotoxicity in vitro was measured by performing methyl thiazolyl tetrazolium (MTT) assay of the HeLa cells incubated with the particles. MTT assay is a standard test for determining the cytotoxicity of materials based on the formation of dark-red formazan by the metabolically active cells after their exposure to MTT. Cells were first collected and seeded into a 96-well (cell culture) plate with a density of 5×10^4 cells/well and incubated for 24 h at 37 °C under 5% CO_2. Then, the Au@$NaYF_4$:Yb^{3+},Er^{3+} nanocomposites with different concentrations of 0.05, 0.10, 0.20, 0.50, 1.00 and 2.00 mg/mL were added to the culture wells. Cells cultured without materials were chosen as the controls. The cells were maintained at 37 °C under 5% CO_2 incubator. After cultivation, the cells were washed with sterilized phosphate buffered saline (PBS) three times. MTT solution (20 μL, 5 $mg{\cdot}mL^{-1}$) was separated into each well of the plate and incubated for 4 h in dark. MTT was then removed and the water-insoluble formazan was dissolved by adding 150 μL dimethyl sulphoxide (DMSO) to each well. The optical density (OD) of the suspension was measured using an absorbance microplate reader TQuant

(BioTEK, USA) at a wavelength of 490 nm. The results show a cumulative analysis of 3 wells per group. The cell viability was then calculated by the following formula: cell viability (%) =[OD]test/[OD]control × 100. Here, OD test denotes absorbance of test wells, while OD control denotes absorbance of negative control wells.

3 Results and discussion

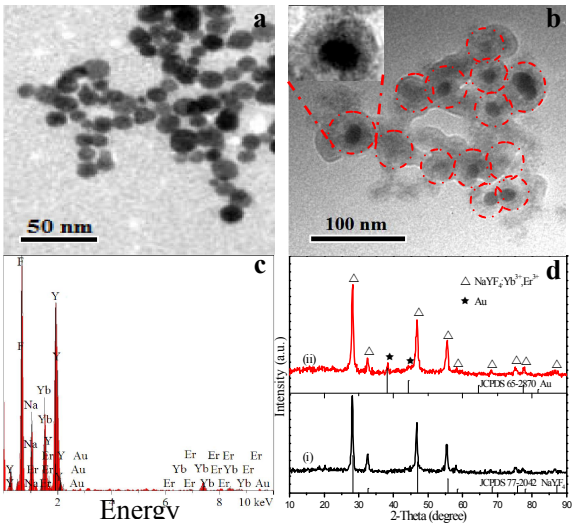

Fig. 1. TEM images of Au nanoparticles (a), Au@$NaYF_4$:Yb^{3+},Er^{3+} nanocomposites (b) (inset is the enlarged TEM image), EDS of Au@$NaYF_4$:Yb^{3+},Er^{3+} nanocomposites (c), XRD patterns of $NaYF_4$:Yb^{3+},Er^{3+} nanocrystals (i) and Au@$NaYF_4$:Yb^{3+},Er^{3+} nanocomposites (ii). The standard card of α-$NaYF_4$ and Au were given as reference (d).

The morphology and size of the Au nanoparticles and Au@$NaYF_4$:Yb^{3+},Er^{3+} nanocomposites were characterized by TEM imaging. The representative TEM image of Au nanoparticles is shown in Fig. 1a. It is noted that Au nanoparticles are roughly spherical in shape and have relatively uniform size with a mean diameter of 15 nm. As evident from Fig. 1b, the TEM image reveals that the $NaYF_4$:Yb^{3+},Er^{3+} nanocrystals with the thickness of 12-20 nm are coated on the surface of Au nanoparticles core layer to form core-shell structures, and the $NaYF_4$:Yb^{3+},Er^{3+} nanoshell layer is not uniform with some aggregated particles appeared. A higher magnification TEM image of a single Au@$NaYF_4$:Yb^{3+},Er^{3+} particle is presented in the inset image of Fig. 1b, in which the core-shell structure is very clear. The Energy dispersive analysis (Fig. 1c) of selected areas of Au@$NaYF_4$:Yb^{3+},Er^{3+} nanocomposites further reveals their elemental composition. The elementals of Y, F, Na, Yb, Er, and Au can be easily detected. The strong peaks of Y, F, Yb, and Na elementals in the EDS spectrum indicate the existence of $NaYF_4$:Yb^{3+},Er^{3+} nanocrystals in the nanocomposites. In addition to these elements, the spectrum also includes the peaks of Au. Those results suggest that the Au@$NaYF_4$:Yb^{3+},Er^{3+} nanocomposites are successfully prepared. The crystalline phases of the as-prepared samples were identified with the X-ray diffraction (XRD) analysis. The XRD patterns of the $NaYF_4$:Yb^{3+},Er^{3+} nanocrystals (i) and Au@$NaYF_4$:Yb^{3+},Er^{3+} nanocomposites (ii) are shown in Fig. 1d. From Fig. 1d(i), it can be seen that the positions of all the diffraction peaks at 28.2°, 32.7°, 46.9°, 55.7°, 75.7° and 87.2° are consistent with the (111), (200), (220), (311), (331) and (422) lattice planes of the standard XRD data for the face-centered cubic phase of $NaYF_4$ (JCPDS card 77-2042). No peaks of any other phases or impurities are detected, indicating that pure α-$NaYF_4$ can be obtained under this condition. The XRD patterns of Au@$NaYF_4$:Yb^{3+},Er^{3+} nanocomposites reveal the presence of diffraction peaks related to cubic-$NaYF_4$ phase. The sample of Au@$NaYF_4$:Yb^{3+},Er^{3+} nanocomposites also exhibit new peaks at 38.2° and 44.6°, which are indexed to (111) and (200) planes of Au diffraction (JCPDS card 65-2870, face-centered). The results indicate the coexistent of Au and α-$NaYF_4$:Yb^{3+},Er^{3+} in the hybrid nanocoposites. More significantly, the weak XRD peaks of Au nanoparticles confirm the growth of $NaYF_4$:Yb^{3+},Er^{3+} shell on the Au nanoparticles core.

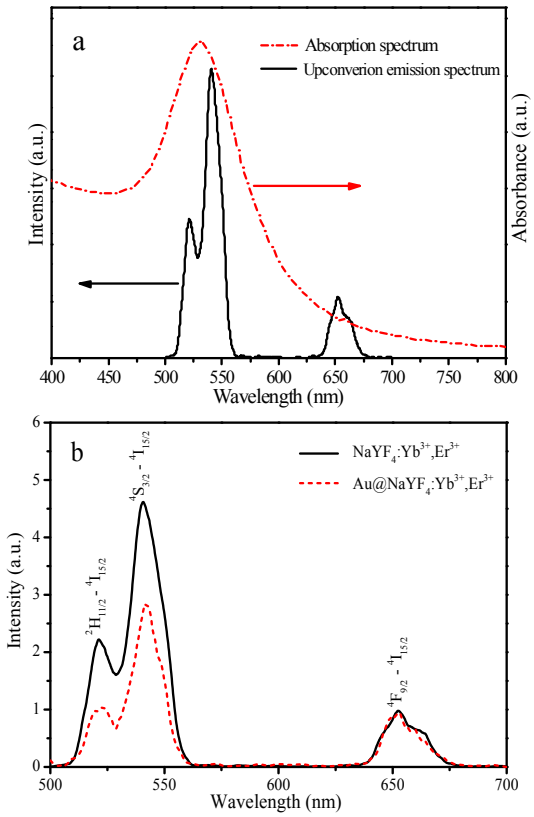

Fig. 2. (a) UV-Vis spectrum of Au nanoparticles in water and upconversion luminescent spectrum of $NaYF_4$:Yb^{3+},Er^{3+} nanocrystals; (b) upconversion luminescent spectra of the $NaYF_4$:Yb^{3+},Er^{3+} nanocrystals and Au@$NaYF_4$:Yb^{3+},Er^{3+} nanocomposites

Fig. 2a displays the UV-Vis absorption spectrum of Au nanoparticles in DI water and the upconversion luminescent spectrum of $NaYF_4$:Yb^{3+},Er^{3+} nanocrystals under 980 nm laser excitation. A strong absorption band at 530 nm is ascribed to the plasmon absorption of Au nanoparticles. From the upconversion emission spectrum of $NaYF_4$: Yb^{3+},Er^{3+} nanocrystals, three main emission bands at 523, 540 and 655 nm are ascribed to the $^2H_{11/2}$-$^4I_{15/2}$, $^4S_{3/2}$-$^4I_{15/2}$ and $^4F_{9/2}$-$^4I_{15/2}$ transitions of Er^{3+} ions. It is noted that the emission peaks of Er^{3+} ions are well overlapped with the

absorption spectrum of Au, satisfying the prerequisite for efficient LRET. To further investigate the energy transfer in the hybrid nanocomposites, we compare the optical property of the $NaYF_4$:Yb^{3+},Er^{3+} nanocrystals with Au@$NaYF_4$:Yb^{3+},Er^{3+} nanocomposites. As shown in Fig. 2b, the positions of the upconversion emission peaks in core-shell structures are accordance with the pure $NaYF_4$:Yb^{3+},Er^{3+} nanocrystals, indicating the upconversion processes from Yb^{3+} to Er^{3+} ion have not been changed through conjugation with Au nanoparticles. We also observe that the intensities of the green upconversion emissions corresponded to $^2H_{11/2}$-$^4I_{15/2}$ and $^4S_{3/2}$-$^4I_{15/2}$ transitions in the $NaYF_4$:Yb^{3+},Er^{3+} nanocrystals are decreased dramatically when the Au nanoparticles are introduced into the hybrid nanocomposites. But that of the red emission assigned to $^4F_{9/2}$-$^4I_{15/2}$ transition is almost not changed. In Fig. 3 for $NaYF_4$: Yb^{3+},Ho^{3+}, an intense green emission at 537 nm and a red emission at 643 nm originate from the $^5S_2$/$^5F_4$-$^5I_8$ and $^5F_5$-$^5I_8$ transitions of Ho^{3+} ions, respectively. The plasmon resonance absorption band around 530 nm of the gold nanoparticles overlaps stronger with the green emission park of Ho^{3+} ions in the $NaYF_4$: Yb^{3+},Ho^{3+} nanocrystals. As seen from the upconversion emission spectra of Au@$NaYF_4$: Yb^{3+},Ho^{3+} in Fig. 3b, the characteristic transitions of the corresponding Ho^{3+} ions can be emitted. However, the upconversion emission intensities of the $^5S_2$/$^5F_4$-$^5I_8$ transitions of Ho^{3+} ions dramatically change. The analysis above shows that the green emission of Au@$NaYF_4$:Yb^{3+},Er^{3+}/Ho^{3+} nanocomposites is obviously quenched in presence of Au nanoparticles. Compared to the green emission, the red emission is almost unchanged. If the results

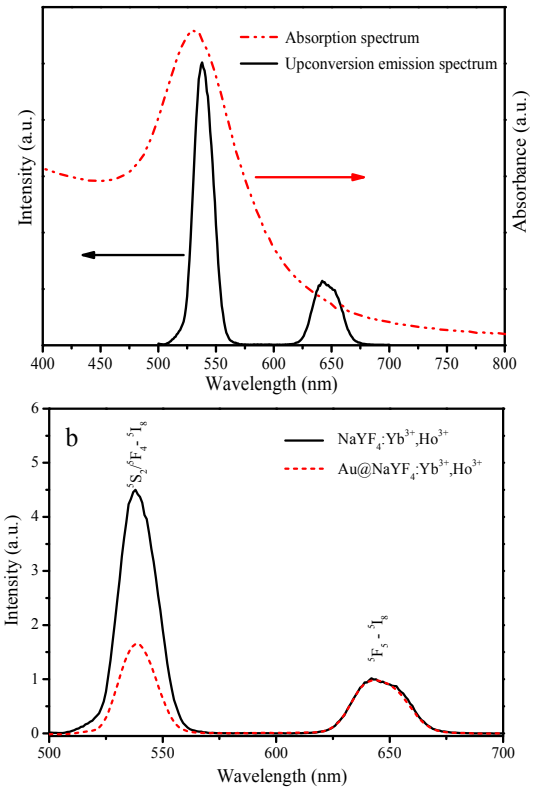

Fig. 3. (a) UV-Vs spectrum of Au nanoparticles in water and upconversion luminescent spectrum of $NaYF_4$:Yb^{3+},Ho^{3+} nanocrystals; (b) upconversion luminescent spectra of the $NaYF_4$:Yb^{3+},Ho^{3+} nanocrystals and Au@$NaYF_4$:Yb^{3+},Ho^{3+} nanocomposites

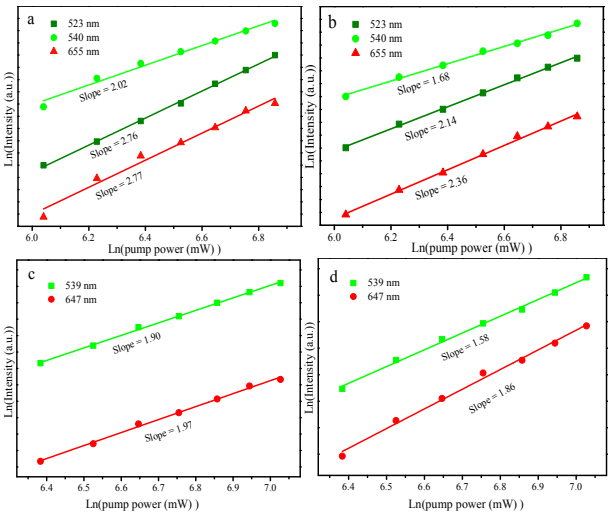

Fig. 4 The Ln–Ln plot of the upconversion emissions intensities as a function of the infrared excitation pump power for $NaYF_4$:Yb^{3+},Er^{3+} nanocrystals(a), Au@$NaYF_4$:Yb^{3+},Er^{3+} nanocomposites(b), $NaYF_4$:Yb^{3+},Ho^{3+} nanocrystals(c), Au@$NaYF_4$:Yb^{3+},Ho^{3+} nanocomposites(d)

depend on the excitation rate, the intensity ratio of green emission and the red emission should be unchanged. Therefore, it is suggested that the resonant excitation and the reduction of excitation rate are ruled out, and the process was mainly due to the non-radiative LRET effect for the spectra overlaps of green emission bands of $NaYF_4$:Yb^{3+},Er^{3+}/Ho^{3+} and the absorption of Au nanoparticles.

To further understand the effect of Au nanoparicles, the dependence of pumping power on the upconversion luminescence intensity is investigated. For the upconversion mechanism, the number of photons required to populate the upper emitting state under unsaturated condition can be described by the following relationship:[7] $I_{up}=KP^n$, where I_{up} is the upconversion luminescence intensity, K is material-related coefficient, P is the infrared excitation pump power, and n is the number of pump photons required. Fig. 4 shows the Ln-Ln plot of the upconversion emissions intensities as a function of the infrared excitation pump power for $NaYF_4$:Yb^{3+},Er^{3+}/Ho^{3+} and Au@$NaYF_4$:Yb^{3+},Er^{3+}/Ho^{3+}, in which the slope indicates the number of photons involved in the upconversion process. The Ln-Ln plot can be fitted well with a line function. The slope values for the $^2H_{11/2}$-$^4I_{15/2}$ (523 nm), $^4S_{3/2}$-$^4I_{15/2}$ (540 nm) and $^4F_{9/2}$-$^4F_{15/2}$ (655 nm) transitions emissions of Er^{3+} ions are 2.76, 2.02 and 2.77, respectively. This illustrates that the 540 nm emission is more likely to involve two photons in the upconversion process and both the 523 and 655 nm emission are three photons processes. When introducing Au nanoparticles, the slope values for the transition emissions of Er^{3+} ions are smaller than those of $NaYF_4$:Yb^{3+},Er^{3+} nanocrystals. From the power dependence plots of $NaYF_4$:Yb^{3+},Ho^{3+}, the upconversion emissions observed at 539 and 647 nm require two photons excitation processes. However, when introducing Au nanoparticles into the system, the slopes for the green and red emission curves of Au@$NaYF_4$:Yb^{3+},Ho^{3+} nanocomposites reduce to 1.58 and 1.86, respectively. The change is similar to the case of the Au@$NaYF_4$:Yb^{3+},Er^{3+} nanocomposites shown as above. From the mechanism discussed

above, the result suggests that the existence of Au nanoparticles can also modify the upconversion processes. Under a 980 nm laser excitation, partial energy is used for upconversion luminescence from the $NaYF_4$:Yb^{3+},Er^{3+}/Ho^{3+} nanocrystals and the other maybe transfer from the $NaYF_4$:Yb^{3+},Er^{3+}/Ho^{3+} nanocrystals to Au nanoparticles in the Au@$NaYF_4$:Yb^{3+},Er^{3+}/Ho^{3+} nanocomposites.

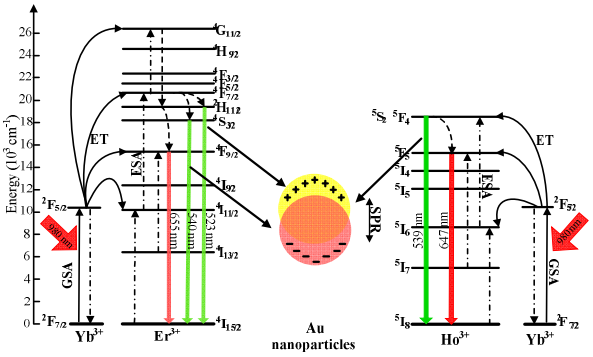

Fig. 5. Schematic illustration of the LRET process, with $NaYF_4$:Yb^{3+},Er^{3+}/Ho^{3+} nanocrystals as energy donors and Au nanoparticles as energy acceptors.

Fig. 5 shows the possible mechanism of upconversion luminescence of $NaYF_4$:Yb^{3+},Er^{3+}/Ho^{3+} nanocrystals and the LRET process between $NaYF_4$:Yb^{3+},Er^{3+}/Ho^{3+} and Au nanoparticles. Under the 980 nm laser excitation, the Yb^{3+} ion is excited to the $^2F_{5/2}$ level from the ground state $^2F_{7/2}$ level in $NaYF_4$:Yb^{3+},Er^{3+}/Ho^{3+} nanocrystals. Due to energy transfer from Yb^{3+} ions , ground and excited state absorption, the Er^{3+} ions are excited to $^4G_{11/2}$ level. With the help of non-radiation transition processes, the electron in the level of $^4F_{7/2}$ decays to the level of $^2H_{11/2}$, $^4S_{3/2}$, or $^4F_{9/2}$ of Er^{3+} ions. Subsequent radiation transitions of the each level to $^4I_{15/2}$ level, the green and red emissions are observed. In addition, Ho^{3+} ions are excited to $^5S_2$/$^5F_4$ level in $NaYF_4$:Yb^{3+},Ho^{3+} nanocrystals through energy transfers from Yb^{3+} ions. We can see the $^5S_2$/$^5F_4$-$^5I_8$ for green emission at 539 nm and $^5F_3$-$^5I_8$ for red emission at 647 nm. For Au@$NaYF_4$:Yb^{3+},Er^{3+}/Ho^{3+} nanocomposites, the donor of $NaYF_4$:Yb^{3+},Er^{3+}/Ho^{3+} nanocrystals and the acceptor of Au nanoparticles are close enough and possess the amount of spectral overlap. Therefore, the emission of the Er^{3+}/Ho^{3+} ions in $NaYF_4$:Yb^{3+},Er^{3+}/Ho^{3+} nanocrystals will be quenched and the energy transfers to Au nanoparticles in the LRET systems. Au nanoparticles as energy acceptor will convert energy to heat and the heat will greatly be useful in photothermal therapy.

To prove the photothermal effect of the Au@$NaYF_4$:Yb^{3+},Er^{3+}/Ho^{3+} nanocomposites, we examine the temperature change of Au@$NaYF_4$:Yb^{3+},Er^{3+}/Ho^{3+} aqueous solution with the 980 nm laser irradiation. From Fig. 6, we observe that the solution temperature can significantly increase at power density of 1.2 W/cm^2 for 10 min. When the 980 nm laser irradiated 10 min, the temperature of aqueous solution of Au@$NaYF_4$:Yb^{3+},Er^{3+} nanocomposites with 100 μg·mL^{-1} is increased from 24.0 °C to 45.0 °C (Fig. 6a). In comparison, the temperature of the water and the $NaYF_4$:Yb^{3+},Er^{3+} aqueous solution have only increased to 31.0 °C and 34.9 °C, respectively. However, the temperature of the Au solutions rises from 21.0 to 41 °C, confirming that the temperature of the solution increment results mainly from Au and slightly from $NaYF_4$:Yb^{3+},Er^{3+} (Fig.6a).The temperature of the aqueous solution with various

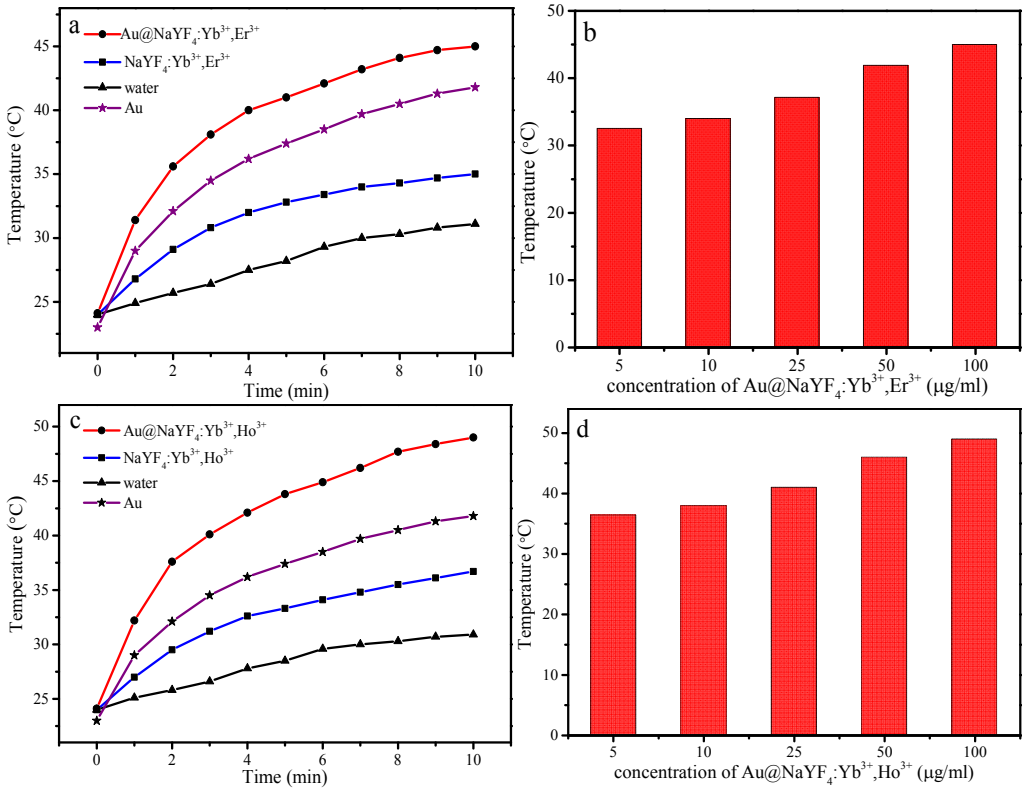

Fig. 6 Photothermal properties of Au@$NaYF_4$:Yb^{3+},Er^{3+} (a,b) and Au@$NaYF_4$:Yb^{3+},Ho^{3+} (c,d) nanocomposites under 980 nm laser irradiation at 1.2 W

concentrations of Au@$NaYF_4$:Yb^{3+},Er^{3+} was also investigated. As the concentration of Au@$NaYF_4$:Yb^{3+},Er^{3+} increases from 5 to 100 μg·mL^{-1}, the obvious temperature increment from 31.3 °C to 45.0 °C is found. As shown in Fig. 6c, the maximum temperature of the $NaYF_4$:Yb^{3+},Ho^{3+} aqueous solution is only about 35 °C with a 980 nm NIR laser at power density of 1.2 W/cm^2 for 10 min. In contrast, the temperature of Au@$NaYF_4$:Yb^{3+},Ho^{3+} aqueous solution increases with the extension of irradiation time and reaches 49.2 °C in the focal region during the irradiation of 980 nm laser for 10 min. As the concentration of Au@$NaYF_4$:Yb^{3+},Ho^{3+} nanocomposites increases, an obvious temperature increment is also found (Fig. 6d). These results suggest that the Au@$NaYF_4$:Yb^{3+},Er^{3+}/Ho^{3+} nanocomposites have a prominent photothermal transduction property and the temperature of photothermal transduction can be easily controlled by adjusting the concentration of Au@$NaYF_4$:Yb^{3+},Er^{3+}/Ho^{3+} nanocomposites. Thus , the Au@$NaYF_4$:Yb^{3+},Er^{3+}/Ho^{3+} nanocomposites could act as an efficient photothermal transduction agent.

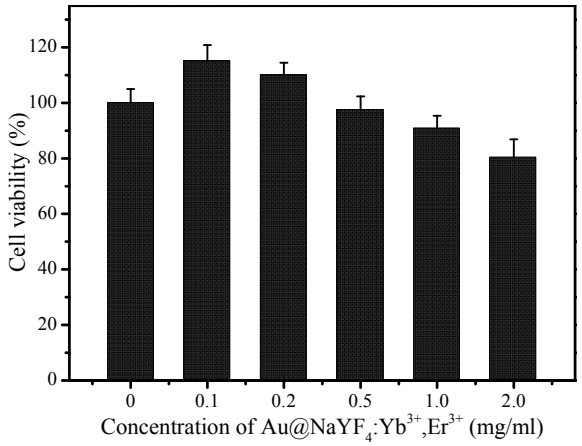

Fig. 7. Cell viability data of HeLa cells after incubation with the Au@$NaYF_4$:Yb^{3+},Er^{3+} at different concentrations for 24 h.

For potential application in biomedicine, the biocompatibility of the Au@$NaYF_4$:Yb^{3+},Er^{3+} nanocomposites is evaluated by the MTT based cytotoxicity assay. Fig. 7 describes the cell viability of Au@NaYF4:Yb^{3+},Er^{3+} at the concentrations of 0.1, 0. 2, 0.5, 1.0, and 2.0 mg/mL incubated for 24 h. It is obviously shown the relatively small variation in cell viability even at high concentrations of the samples, indicating that Au@$NaYF_4$:Yb^{3+},Er^{3+} nanocomposites are low cytotoxicity to the living cells. When the concentration of Au@$NaYF_4$:Yb^{3+},Er^{3+} nanocomposites increased to 2.0 mg·mL^{-1}, the cell viability is more than 85.7%. MTT assay results suggest that the Au@$NaYF_4$:Yb^{3+},Er^{3+} nanocomposites have a good biocompatibility and can be promising applied in biomedicine.

4 Conclusions

In summary, the bifunctional hybrid nanocomposites have been prepared combining $NaYF_4$:Yb^{3+},Er^{3+}/Ho^{3+} nanocrystals and Au nanoparticles via a facile solution route. The Au nanoparticles were coated by $NaYF_4$:Yb^{3+},Er^{3+}/Ho^{3+} nanocrystals, which were confirmed by TEM measurements. The shell layer can provide an efficient upconversion luminescence. Meanwhile, we observe the overlap between the absorption band of Au nanoparticles and the upconversion emission peaks of the Er^{3+} ions or Ho^{3+} ions in $NaYF_4$:Yb^{3+},Er^{3+}/Ho^{3+} nanocrystals. The LRET system is developed using $NaYF_4$:Yb^{3+},Er^{3+}/Ho^{3+} nanocrystals serve as energy donor and Au nanoparticles as energy acceptor. The upconversion luminescence intensities of Er^{3+}/Ho^{3+} ions are investigated under the different pumping power. The results show that the number of photons involved in the upconversion process of the samples is decreased and the highly efficient LRET may be occurred from the $NaYF_4$:Yb^{3+},Er^{3+}/Ho^{3+} nanocrystals to Au nanoparticles in the nanocomposites. Under 980 nm laser irradiation, the efficient photothermal behavior of the hybrid nanocomposite is found. The solution temperature can significantly increase. The temperature of aqueous solution with 100 μg·mL^{-1} Au@$NaYF_4$:Yb^{3+},Er^{3+} and Au@$NaYF_4$:Yb^{3+},Ho^{3+} nanocomposites is increased to 45.0 °C and 49.2 °C, respectively. Moreover, the temperature of photothermal transduction can be easily controlled by adjusting the concentration of Au@$NaYF_4$:Yb^{3+},Er^{3+}/Ho^{3+} nanocomposites. Additionally, the Au@$NaYF_4$:Yb^{3+}, Er^{3+} nanocomposites have low toxicity and good biocompatibility, significantly facilitating biomedical application. It is also expected that the Au@$NaYF_4$:Yb^{3+},Er^{3+}/Ho^{3+} nanocomposites realize upconversion imaging and photothermal therapy in the biomedical fields.

Acknowledgment

This work was financially supported by the National Natural Science Foundation of P.R. China (NSFC) (Grant No. 51072026, 50972020) and the Development of science and technology plan projects of JiLin province (Grant No. 20130206002GX)

Notes and references

[a] *Key Laboratory of Applied Chemistry and Nanotechnology at Universities of Jilin Province, Changchun University of Science and Technology, Changchun 130022, P. R. China.* Tel.:+86-431-85582574. Fax.: +86-431-85383815; E-mail address: liuguixia22@163.com
[b] *College of Life Science, Changchun University of Science and Technology, Changchun 130022, P. R. China*

1 F. Wang, Y. Han, C. S. Lim, Y. Lu, J. Wang, J. Xu, H. Chen, C. Zhang, M. Hong, X. Liu, *Nature*, 2010, **463**, 1061-1065.
2 F. Wang, X. Liu, *Accounts Chem. Res.*, 2014, **47**, 1378-1385.
3 T. Liu, X. Bai, C. Miao, Q. Dai, W. Xu, Y. Yu, Q. Chen, H. Song, *J. Phys. Chem. C*, 2014, **118**, 3258-3265.
4 L. D. Sun, Y. F. Wang, C. H. Yan, *Accounts Chem. Res.*, 2014, **47**, 1001-1009.
5 H. Na, K. Woo, K. Lim, H. S. Jang, *Nanoscale*, 2013, **5**, 4242-4251.
6 Y. Liu, D. Tu, H. Zhu, X. Chen, *Chem. Soc. Rev.*, 2013, **42**, 6924-6958.
7 G. Chen, H. Qiu, P. N. Prasad, X. Chen, *Chem. Rev.*, 2014, **114**, 5161-5214.
8 P. Qiu, N. Zhou, H. Chen, C. Zhang, G. Gao, D. Cui, *Nanoscale*, 2013, **5**, 11512-11525.
9 A. Gnach, A. Bednarkiewicz, *Nano Today,* 2012, **7**, 532-563.
10 R. Lv, S. Gai, Y. Dai, N. Niu, F. He, P. Yang, *ACS Appl. Mater. Inter.*, 2013, **5**, 10806-10818.
11 C. Li, J. Lin, *J. Mater. Chem.*, 2010, **20**, 6831-6847.
12 D. J. Gargas, E. M. Chan, A. D. Ostrowski, S. Aloni, M. V. P. Altoe, E. S. Barnard, B. Sanii, J. J. Urban, D. J. Milliron, B. E. Cohen, P. J.

Schuck, *Nat Nano*, 2014, **9**, 300-305.
13 H. Chen, L. Shao, Q. Li, J. Wang, *Chem. Soc. Rev.*, 2013, **42**, 2679-2724.
14 M. Eguchi, D. Mitsui, H. L. Wu, R. Sato, T. Teranishi, *Langmuir*, 2012, **28**, 9021-9026.
15 R. Jiang, B. Li, C. Fang, J. Wang, *Adv. Mater.*, 2014, **26**, 5274-5309.
16 L. Dykman, N. Khlebtsov, *Chem. Soc. Rev.*, 2012, **41**, 2256-2282.
17 J. Lin, S. Wang, P. Huang, Z. Wang, S. Chen, G. Niu, W. Li, J. He, D. Cui, G. Lu, X. Chen, Z. Nie, *ACS Nano*, 2013, **7**, 5320-5329.
18 M. Eichelbaum, K. Rademann, *Adv. Funct. Mater.*, 2009, **19**, 2045-2052.
19 W. Xu, S. Xu, Y. Zhu, T. Liu, X. Bai, B. Dong, L. Xu, H. Song, *Nanoscale*, 2012, **4**, 6971-6073.
20 F. Cao, R. Deng, D. Liu, S. Song, S. Wang, S. Su, H. Zhang, *Dalton Trans*, 2011, **40**, 4800-4802.
21 J. Liao, Z. Yang, S. Lai, B. Shao, J. Li, J. Qiu, Z. Song, Y. Yang, *J. Phys. Chem. C*, 2014, **118**,17992-17999.
22 Z. Li, L. Wang, Z. Wang, X. Liu, Y. Xiong, *J. Phys. Chem. C*, 2011, **115**, 3291-3296.
23 F. Zhang, G. B. Braun, Y. Shi, Y. Zhang, X. Sun, N. O. Reich, D. Zhao, G. Stucky, *J. Am. Chem. Soc.*, 2010, **132**, 2850-2851.
24 L. Sudheendra, V. Ortalan, S. Dey, N. D. Browning, I. M. Kennedy, *Chem. Mater.*, 2011, **23**, 2987-2993.
25 P. Yuan, Y. H. Lee, M. K. Gnanasammandhan, Z. Guan, Y. Zhang, Q. H. Xu, *Nanoscale,* 2012, **4**, 5132-5137.
26 M. Saboktakin, X. Ye, S. J. Oh, S. H. Hong, A. T. Fafarman, U. K. Chettiar, N. Engheta, C. B. Murray, C. R. Kagan, *ACS Nano*, 2012, **6**, 8758-8766.
27 A. Priyam, N. M. Idris, Y. Zhang, *J. Mater. Chem.*, 2012, **22**, 960-965.
28 P. Reineck, D. Gómez, S. H. Ng, M. Karg, T. Bell, P. Mulvaney, U. Bach, *ACS Nano*, 2013, **7**, 6636-6648.
29 M. Fujii, T. Nakano, K. Imakita, S. Hayashi, *J. Phys. Chem. C*, 2012, **117**, 1113-1120.
30 P. Anger, P. Bharadwaj, L. Novotny, *Phys. Rev. Lett*, 2006, **96**, 113002.
31 H. Zhang, Y. Li, I. A. Ivanov, Y. Qu, Y. Huang, X. Duan, *Angew. Chem.*, 2010, **122**, 2927-2930.
32 D. Darvill, A. Centeno, F. Xie, *Phys. Chem. Chem. Phys.*, 2013, **15**, 15709-15726.
33 C. J. Breshike, R. A. Riskowski, G. F. Strouse, *J. Phys. Chem. C*, 2013, **117**, 23942-23949.
34 Y. Song, G. Liu, J. Wang, X. Dong, W. Yu, *Phys. Chem. Chem. Phys.*, 2014, **16**, 15139-15145.
35 M. Ray, T. S. Basu, N. R. Bandyopadhyay, R. F. Klie, S. Ghosh, S. O. Raja, A. K. Dasgupta, *Nanoscale,* 2014, **6**, 2201-2210.
36 J. Q. Gu, L. D. Sun, Z. G. Yan, C. H. Yan, *Chem.-Asian J*, 2008, **3**, 1857-1864.
37 W. W. Ye, M. K. Tsang, X. Liu, M. Yang, J. Hao, *Small,* 2014, **10**, 2390-2397.
38 Z. Wang, L. Wu, B. Shen, Z. Jiang, *Talanta,* 2013, **114**, 124-130.